Journal of Petroleum Science and Engineering 204 (2021) 108753

Contents lists available at ScienceDirect

Journal of Petroleum Science and Engineering

journal homepage: http://www.elsevier.com/locate/petrol

A review on proppant transport modelling

Beatriz Ramos Barboza [a], Bin Chen [a,b], Chenfeng Li [a,c,*]

[a] Zienkiewicz Centre for Computational Engineering, College of Engineering, Swansea University Bay Campus, Swansea, SA1 8EN, United Kingdom
[b] Energy Geosciences Division, Lawrence Berkeley National Laboratory, Berkeley, CA, 94720, USA
[c] Energy Safety Research Institute, College of Engineering, Swansea University Bay Campus, Swansea, SA1 8EN, United Kingdom

ARTICLE INFO

Keywords:
Proppant transport
Hydraulic fracturing
Multiphase flow
Numerical simulation

ABSTRACT

Proppant transport is a critical physical process in hydraulic fracturing which has been extensively used for reservoir stimulation in petroleum engineering. Proppants injected together with fracturing fluid provide structural support to the stimulated fracture network and prevent them from closing after flowback. Hence, the final proppant distribution in fracture networks affects directly the effectiveness of hydraulic fracturing. Owing to the limitation and high cost of well logging, computational modelling has been increasingly used to study proppant transport, where different assumptions and numerical models have been employed often without rigorous validation or justification. This work presents a comprehensive review on proppant transport modelling, from relevant physics to numerical approaches, aiming to provide an unbiased global picture of the-state-of-the-art studies, inspire new insights, and promote the development of innovative and reliable computational models for proppant transport.

1. Introduction

Hydraulic fracturing (also known as hydrofracking or fracking) is a technique to create fluid-driven fracture networks in tight formations and thereby increase the formation permeability of unconventional oil and gas reservoirs. Since the first hydraulic fracturing operation conducted in 1947 on a gas well in the Hugoton field (USA) (Hubbert and Willis, 1957; Carter et al., 2000; Adachi et al., 2007), the application has been growing continuously and is now widely used by the petroleum industry for reservoir stimulation, thereby enhancing the production of oil or natural gas (Detournay, 2016; Obeysekara, 2018; Chen et al., 2020). As shown in Fig. 1, hydraulic fracturing is a coupled process involving rock deformation, fluid flow, and the dynamic fracture propagation (Vandamme and Curran, 1989; Vandamme et al., 1989; Rahman and Rahman, 2010; Mokryakov, 2011; Lavrov, 2017; Chen et al., 2018a, b,). During the injection stage the fracture area grows, but if the pumping stops it may close, loosing the newly created flow paths (Barati and Liang, 2014). Hence, proppants (small particles like sand) are usually added into the fracturing fluid to be carried into the fracture as a slurry (i.e. mixture of pulverized solids and a liquid). Then, in the ideal scenario, the fracturing fluid flows back to the wellbore after pumping ends and the proppant particles stay in place to prevent fractures from closing and preserve the created flow path during the production phase (Babcock et al., 1967; Adachi et al., 2007; Dontsov and Peirce, 2014b; Wu et al., 2014; Sahai and Moghanloo, 2019). Therefore, the final distribution of proppant in the stimulated fracture network is critical to the effective fracture network (Kong et al., 2015).

The final distribution of proppant in the stimulated fracture network is determined jointly by the injection strategies, properties of proppant and fracturing fluid, complexity of the fracture network, etc. (Blyton et al., 2015; Dogon and Golombok, 2016; Tong and Mohanty, 2016; Hu et al., 2018a; Chang et al., 2018; Sahai and Moghanloo, 2019; Gong et al., 2020). The last several decades have seen a better understanding on the influence of the injection strategies and the development of diverse types of proppant and fracturing fluid. The first batch of fluid injected is usually clean in order to generate larger fracture width (Perkins and Kern, 1961). Then the smaller particle size proppants are injected followed by larger particle size proppants to maximize the near wellbore conductivity (Liang et al., 2016). However, a reverse proppant addition schedule was recommended by Hu et al. (2018a) through numerical simulation. The size of proppant is generally between 8 and 140 mesh (i.e. 105μm – 2.38 mm) (Liang et al., 2016). The types of proppants have been broadened from the silica sand used in the first fracking job (Barati and Liang, 2014; Liang et al., 2016) to such diverse materials as precured resin-coated sand, curable resin-coated sand, intermediate-strength ceramic proppant, lightweight ceramic proppant

* Corresponding author.
E-mail address: c.f.li@swansea.ac.uk (C. Li).

https://doi.org/10.1016/j.petrol.2021.108753
Received 2 August 2020; Received in revised form 30 January 2021; Accepted 30 March 2021
Available online 5 April 2021

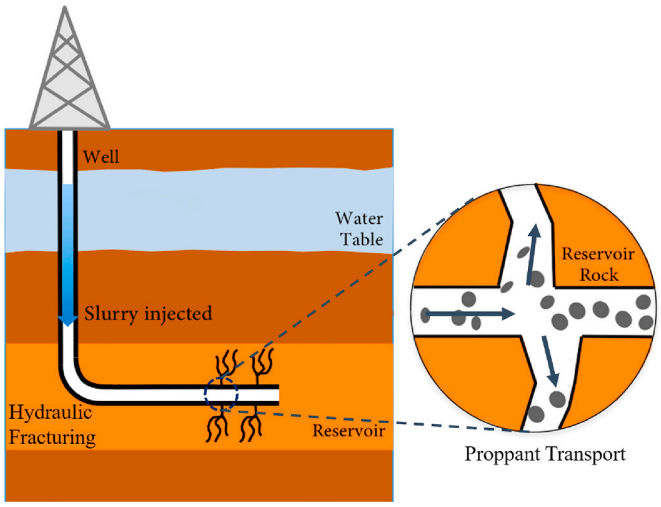

Fig. 1. Proppant transport in hydraulic fracturing process.

and high-strength proppant (Fink, 2013; Zoveidavianpoor and Gharibi, 2015; Liang et al., 2016; Belyadi et al., 2017). The commonly used fracturing fluids for carrying proppants include slickwater, gel and crosslinked fluid etc., whose viscosities vary greatly from 1 cP to over 1000 cP (Fink, 2012; Al-Muntasheri, 2014).

Numerical modelling is an important technique to better understand the relevant mechanisms for proppant transport in hydraulic fracturing and to optimise the designs of proppant, fracturing fluid and injection strategy. The proppant transport in stimulated fracture networks is essentially a multiphase flow system with some unique characteristics, posing several major challenges to its numerical simulation. First, besides the fluid-particle interaction and settling which generally occur in particle-laden flows, other physical processes such as bed formation, screenout and wall effect also need to be carefully considered in proppant transport modelling (Kern et al., 1959; Raimbay et al., 2016). Secondly, instead of taking place within a fixed geometry, the fluid domain of proppant transport keeps changing as the fracture propagates and it forms into irregular paths and complex networks, which significantly increases the numerical challenges of the associated fluid simulation (Chang, 2014; Tong and Mohanty, 2016; Chang et al., 2018; Sahai and Moghanloo, 2019). Thirdly, the large quantity of proppants (several thousand tons) injected in a hydraulic fracturing operation and the significant size difference between proppant (often less than a mm) and hydraulic fracture (several hundred metres) make the high-fidelity simulation of proppant transport extremely expensive, which is further complicated by the dynamic coupling between proppant transport and fracture propagation.

The numerical methods for multiphase flow simulation can be classified into two groups: Eulerian-Eulerian and Eulerian-Lagrangian schemes. Based on both schemes, many numerical models have been proposed to investigate proppant transport during hydraulic fracturing. Some models consider simplified configurations, e.g. a flow channel formed by two parallel plates with fixed height, length and width, while the others (Boronin and Osiptsov, 2010; Blyton et al., 2015; Hu et al., 2018b, a) deal with the entire hydraulic fracture process involving both fracture propagation and proppant transport. For the latter, the main focus has been on the fracture initiation and propagation, while much simplified conditions and models are adopted to model proppant transport. As a result of various assumptions and the lack of accurate formation data, existing hydraulic fracture simulations are often found to over-predict propped or effective fracture lengths by 100%–300% (Blyton et al., 2015).

The purpose of this paper is to provide a dedicated review on the state-of-the-art modelling techniques of proppant transport, focusing on the physical mechanisms behind the phenomenon, relevant theories, and existing proppant transport models. A summary of the advantages and disadvantages of diverse numerical models is provided. The review is divided into two parts: the physics and theories involved in proppant transport and the modelling approaches, which are presented in § 2 and § 3, respectively.

2. The physics behind proppant transport

After a fracture is opened by the fluid pressure, proppants are injected with the fracturing fluid to prevent the hydraulic fracture from closing. The dynamic behaviours of proppant particles throughout the fracture path involve a number of physical processes which are explained in the following subsections.

2.1. Multiphase flow

Since proppant particles are mixed with fracturing fluid and injected together through the fracture, the process of proppant transport can be treated as a multiphase flow system with at least two distinct phases: the liquid and solid particles (Shook and Roco, 1991; Wang et al., 2018a). This kind of slurry flow is commonly encountered in such diverse industries as petroleum, chemical and manufacturing sectors.

It is however not easy to give an exact definition of a multiphase system since it depends on both the physical nature of problem and the investigation approach (Prosperetti and Tryggvason, 2009). A phase can be characterized as a class of materials that has a specific inertial response to the interaction between the phase itself and the flow field in which it is immersed. Hence, the concept of phase in multiphase flow systems is not directly related to material characteristics. For example, particles of the same material with different sizes can be treated as different phases, as their dynamical responses to the flow field differ (Austin et al., 1997; Crowe et al., 2012). For multiphase flow simulation, choosing a correct mathematical model to represent the interphase interaction is critical.

Treating the mixture of proppant and fracturing fluid as a uniformly mixed slurry, its bulk motion in hydraulic fractures can be described by the Navier-Stokes equations (Moukalled et al., 2016):

$$\frac{\partial}{\partial t}(\rho \boldsymbol{v}) + \nabla \cdot (\rho \boldsymbol{v}\boldsymbol{v}) = -\nabla p + \nabla \cdot \boldsymbol{\tau} + \rho \boldsymbol{g} + \boldsymbol{F} \tag{1}$$

$$\frac{\partial \rho}{\partial t} + \nabla \cdot (\rho \boldsymbol{v}) = 0 \tag{2}$$

where ρ is the density of the slurry, $\boldsymbol{v}$ is the slurry velocity, p is fluid pressure, $\boldsymbol{g}$ is gravitational acceleration, $\boldsymbol{F}$ is external forces, $\boldsymbol{\tau}$ is the viscous and turbulent stress tensor and is expressed in following form for Newtonian fluid:

$$\boldsymbol{\tau} = \mu\left(\nabla \boldsymbol{v} + \nabla \boldsymbol{v}^T - \frac{2}{3}\boldsymbol{I}(\nabla \cdot \boldsymbol{v})\right) \tag{3}$$

where μ is the dynamic viscosity of the slurry (see § 2.5 for more detailed discussions) and $\boldsymbol{I}$ the identity tensor. The slurry density ρ is expressed as:

$$\rho = c\rho_p + (1-c)\rho_f \tag{4}$$

where c is the particle concentration, ρ_p the particle density, and ρ_f the fluid density.

The above single-phase Navier-Stokes equations do not distinguish the relative motion between the dispersed proppant phase and the continuous fracturing fluid phase, and as a result such phenomena as proppant settling, bed formation and screenout cannot be captured. A multiphase flow approach is therefore needed. There are two main approaches for proppant transport modelling (Andrews and O'Rourke, 1996; Prosperetti and Tryggvason, 2009; Ansys, 2009): the Eulerian-Eulerian scheme and the Eulerian-Lagrangian scheme. The

main difference between them is how the dispersed phase (i.e. proppants in this study) is treated in the simulation. In the Eulerian-Eulerian approach, both the continuous fracturing fluid phase and the dispersed proppant phase are treated as inter penetrating continua, and their motions can be solved using either the two-fluid model (i.e. two sets of coupled Navier-Stokes equations are solved, one for each phase) or the mixture model (i.e. one set of Navier-Stokes equation is solved to obtain the mixture average, after which the relative motions between each phase and the mixture average are explicitly calculated with an analytical solution). In the Eulerian-Lagrangian approach, the continuous fracturing fluid phase is described by the Navier-Stokes equations, while the dispersed proppant phase is represented by Newton's law (see § 3 for more details).

2.2. Lubrication theory

In the context of hydraulic fracturing, proppant transport takes place inside a domain where width is always much smaller than the height and length, especially in unconventional reservoirs. Based on this geometric condition, the Navier-Stokes equations can be simplified according to the so called lubrication theory (Osiptsov, 2017). The lubrication theory describes a flow in a domain where one dimension is much smaller than the others (Batchelor, 2000), and has been one of the most widely used fluid flow models in various hydraulic fracturing simulators (Economides and Nolte, 2000; Osiptsov, 2017).

The lubrication theory ignores the fluid flow along the smallest dimension. Therefore, when it is used in hydraulic fracturing simulation, the flow perpendicular to fracture wall is ignored, resulting in a 2D model to approximate the 3D Navier-Stokes system (Economides and Nolte, 2000). With the change of fracture width considered, the Navier-Stokes equation (1) reduces to the Poiseuille's law, a partial differential equation that relates the flow velocity to the change of fracture width and the pressure gradient (Adachi et al., 2007)

$$\nabla \cdot \left(\frac{w^3}{12\mu} (\nabla p - \rho \boldsymbol{g}) \right) = \frac{\partial w}{\partial t} \tag{5}$$

where w is the fracture width.

2.3. Settling and convection

Once proppants are injected into the fracture, particles travel until they settle downwards at the bottom of fracture space. Induced by a combination of gravitational, drag and buoyant forces, proppant settling out of suspension has been considered as one of the most important proppant transport mechanisms (Mack et al., 2014; Liang et al., 2016).

The proppant suspension has been commonly described by the Stokes flow model, which assumes proppants as small particles suspended in a low-velocity laminar flow with negligible inertial force (Clark and Quadir, 1981; Shah, 1982). The interaction between carrier fluid and proppant particles is represented by the drag force that acts in the opposite direction of flow, which is typically expressed as a function of the slip velocity between phases. For a Newtonian fluid in the Stokes regime, the drag force can be expressed as (Panton, 1996; Batchelor, 2000):

$$F_D = C_D \frac{\pi}{8} \rho_f d_p^2 v_{slip}^2 \tag{6}$$

where C_D is the drag coefficient, ρ_f the fluid density, d_p the diameter of particles, and v_{slip} the relative velocity. As an empirical parameter, the drag coefficient C_D is often related to the Reynolds number Re:

$$C_D = \frac{24}{Re} \tag{7}$$

$$Re = \frac{d_p \rho_f |v_p - v_f|}{\mu_f} \tag{8}$$

where v_p and v_f denote the particle velocity and fluid velocity, respectively, and μ_f is the fluid viscosity. Therefore, the Reynolds number directly affects the terminal velocity of falling particles (Clark and Quadir, 1981). For example, with a low Reynolds number ($Re \leq 2$), the terminal settling velocity for a single particle induced by gravity in an infinitely large space can be obtained as (Novotny, 1977):

$$v_{inf} = \frac{g d_p^2 (\rho_p - \rho_f)}{18 \mu_f} \tag{9}$$

where ρ_p denotes the particle density. According to (Mack et al., 2014), Eq. (9) is also applicable to fracturing fluids of viscosity range between 50 cP and 100 cP. When the Reynolds number Re increases to $2 \sim 500$, the settling velocity is better described by Eq. (10) and Eq. (11); and when Re exceeds 500, the settling velocity is better represented by Eq. (12) and Eq. (13).

$$v_{inf} = \left(\frac{0.072 (\rho_p - \rho_f) g \cdot d_p^{1.6}}{\rho_f^{0.4} \mu_f^{0.6}} \right)^{0.71} \tag{10}$$

$$C_D = \frac{18.5}{Re^{0.6}} \tag{11}$$

$$v_{inf} = \sqrt{\frac{(\rho_p - \rho_f) g d_p^2}{0.33 \rho_f}} \tag{12}$$

$$C_D = 0.44 \tag{13}$$

The above equations are developed for a single particle settling. As the fluid phase of slurry leaks into the formation, the proppant concentration increases, which can then affect proppant settling (Babcock et al., 1967; Novotny, 1977; Clark and Quadir, 1981; Meehan et al., 1991). A hindered proppant settling occurs when particles are close to each other such that their motions are restricted by neighbouring particles. A relationship given by Clark and Quadir (1981) is listed as:

$$v_s = v_{inf} \frac{c}{10^{1.82(1-c)}} \tag{14}$$

where v_s is the corrected settling velocity, and c proppant concentration.

Gadde et al. (2004) proposed another empirical correlation to model the reduction of the settling velocity of proppant with the proppant concentration c approaches the pack limit as:

$$v_s = v_{inf} (2.37c^2 - 3.08c + 1) \tag{15}$$

Apart from the settling mechanism discussed above, Cleary et al. (1991) and Cleary and Amaury Fonseca (1992) introduced the term "convection" to represent a mass of injected slurry moving at the bottom of fracture due to the density difference between injected mixture and pad fluid, resulting in a downward motion. Fig. 2 shows a mass of slurry moving down due to the contact with the fluid preciously present in the

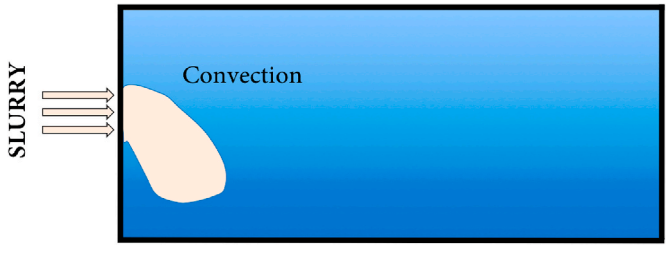

Fig. 2. Schematic of convection during proppant transport.

geometry. Convection is related to the vertical motion of particles. However, instead of being governed by the slippage between fracturing fluid and proppant particles, convection is directed by the bulk density disparity (Mobbs and Hammond, 2001). More recently, the proppant settling behaviour was also related to the fluid characteristics by Clark (2006), where the carrier fluid is classified into two groups: crosslinked and non-crosslinked. It is concluded that proppant settling can occur in non-crosslinked fluids but not in crosslinked fluids.

2.4. Wall effect

Due to the small width of hydraulic fractures, proppant transport is likely to be affected by the fracture wall causing bridging, clogging or trapping of particles. To consider these effects on proppant settling, Novotny (1977) introduced a fracture wall coefficient f_w for $Re < 1$ and $Re > 100$ as follows:

$$f_w = \frac{v_w}{v_{inf}} = \begin{cases} 1 - 0.6526\left(\frac{d_p}{w}\right) + 0.147\left(\frac{d_p}{w}\right)^3 - 0.131\left(\frac{d_p}{w}\right)^4 - 0.0644\left(\frac{d_p}{w}\right)^5, Re < 1 \\ 1 - \left(\frac{d_p}{2w}\right)^{\frac{3}{2}}, Re > 100 \end{cases} \tag{16}$$

where v_w is the corrected settling velocity accounting for the wall effect and v_{inf} is the settling velocity of single particle. For cases between these two regions, a simple linear interpolation based on the Reynolds number is used.

Instead of distinguishing the flow regime with Reynolds number, Liu et al. (2005) proposed to use the particle radius r_p and the half width of fracture w_h to represent the wall effect:

$$f_w = \frac{v_w}{v_{inf}} = \begin{cases} 1 - 0.16\mu_f^{0.28}\frac{r_p}{w_h}, \frac{r_p}{w_h} < 0.9 \\ 8.26 \cdot e^{-0.0061\mu_f}\left(1 - \frac{r_p}{w_h}\right), \frac{r_p}{w_h} \geq 0.9 \end{cases} \tag{17}$$

where μ_f denotes the viscosity of Newtonian fluids or apparent viscosity for Non-Newtonian fluids.

It is worth to note that besides the small width, wall roughness also impacts proppant transport (Huitt, 1956; Wahl and Campbell, 1963; Suri et al., 2020a). Huitt (1956) and Wahl and Campbell (1963) highlighted that in regions of turbulent flow roughness effects become prominent. Additionally, as suggested by Liu et al. (2005); Huang et al. (2019); Suri et al. (2019, 2020a), there is a significant difference between proppant movement in a smooth vertical fracture compared to in a rough one, which affects the final settling and bank location. Liu et al. (2005) demonstrated how much wall roughness retards particles velocity. Fingering of slurry is created when roughness becomes large and to overcome the fingering issue, an injection of a low-viscous fluid after the high viscous slurry is recommended, which carries proppants deeper into the fracture. This technique is named Reverse-Hybrid Frac (Liu et al., 2007). Raimbay et al. (2016) pointed out that surface roughness also affects the placement stability of proppants. Thus, in a smooth wall model, particles get distributed more uniformly and packed as multi-layers, while in rough fractures, particles get distributed non-uniformly and formed a partial-monolayer.

2.5. Slurry viscosity

Proppants are injected into the fracture as a mixture with fracturing fluid and move downwards and settle at the bottom of the fracture due to gravity. The settling rate is dependent on fracturing fluid, fracture characteristics as well as particle behaviour, which can also affect slurry properties. Any variation of proppant concentration during proppant transport directly affects the viscosity of slurry in the region (Barree and Conway, 1995; Dogon and Golombok, 2016). Besides proppant concentration, the particle-particle and particles-fluid interactions also affect the slurry viscosity (Gillies et al., 1999). Hence, to determine the effective viscosity of the slurry is critical for proppant transport modelling (Shah, 1982; Hammond, 1995).

There have been numerous empirical models proposed in the literatures to estimate the effective viscosity of slurry. The first viscosity estimation for a suspension fluid is arguably proposed by Einstein (1905), which simply relates the slurry viscosity of dilute flows with the particle concentration:

$$\mu = \mu_f(1 + 2.5c) \tag{18}$$

The above estimation assumes a uniform distribution of large particles at low concentration. There have been a number of variations to this simple estimation. For example, Nicodemo et al. (1974) proposed:

$$\mu = \mu_f\left(1 + \frac{1.25c}{1 - \frac{c}{c_{\max}}}\right)^2 \tag{19}$$

where μ_f is the Newtonian effective viscosity of the clean fluid, and $c_{\max}$ is maximum volume fraction for the packing. Another similar variation was proposed by Adachi et al. (2007); Boronin and Osiptsov (2010):

$$\mu = \mu_f\left(1 - \frac{c}{c_{\max}}\right)^{\beta} \tag{20}$$

where β is a negative number normally between -3 and -1. In Eq. (19) and Eq. (20), the slurry viscosity tends to infinity when the particle concentration approaches the maximum packing limit. Therefore, a threshold value is generally enforced on the slurry viscosity to avoid numerical instability in numerical modelling of proppant transport.

Besides the above Einstein-type estimations, other forms of slurry viscosity formulae have also been proposed, such as

$$\mu = 1.125\mu_f\left(\frac{\left(\frac{c}{c_{\max}}\right)^{\frac{1}{3}}}{1 - \left(\frac{c}{c_{\max}}\right)^{\frac{1}{3}}}\right) \tag{21}$$

proposed by Frankel and Acrivos (1967) and

$$\mu = \mu_f\left(1 + 2.5c + 10.05c^2 + 0.00273\exp(16.6c)\right) \tag{22}$$

proposed by Thomas (1965).

It should be noted that all aforementioned estimations are empirical or based on oversimplified assumptions. To date, there has not been a general consensus on the effective viscosity of slurry. Based on kinetic theory of granular flows, Eskin and Miller (2008) proposed a computational model for a non-Newtonian slurry convection in a small fracture domain. Their model takes into account particle collision and ideal-gas motion, and the slurry viscosity is calculated as (Shook and Roco, 1991):

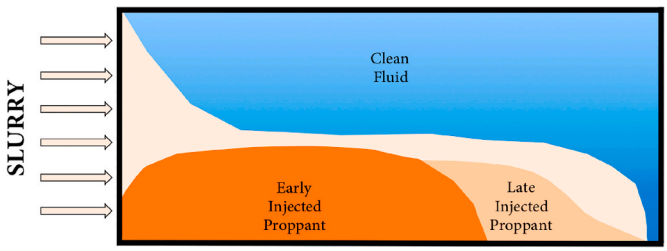

Fig. 3. Schematic for proppant bed formation.

$$\mu = \mu_f\left(1 + 2.5c + 10.05c^2 + 0.0019\exp(20c)\right) \tag{23}$$

2.6. Bed formation

As shown in Fig. 3, an immobile proppant bed can form at the bottom of the fracture during the proppant injection stage (Kern et al., 1959; Patankar et al., 2002). The proppant bed formation is more likely to occur when thin fracturing fluids are used, since the low viscosity fracturing fluid carries less particles to the fracture tip and proppants may settle more quickly near the wellbore. The height of proppant bank tends to grow continuously until it reaches an equilibrium threshold, determined by the velocity of fluid flowing across the top of the bank (Hu et al., 2018b). An early-stage deposition causes accumulation of proppants at the beginning of the fracture and is problematic for practical hydraulic fracturing operations.

After the formation of proppant bed, the bank settling movement will dominate the transport of particles. The initiation of particle movement from the bed is determined by the unbalance of forces acting on the particles. The forces exerting on proppants can be generally grouped into four types: drag, lift, gravity and buoyancy. The drag force is parallel to the fluid flow, the lift force is normal to the proppant bed, and the sum of gravity and buoyancy tends to act downwards. The movement of particles from the bed is closely related to the carrier fluid flow. According to (Mack et al., 2014), if the velocity of the carrier fluid passing over the proppant bed is low, few particles are moved. If the fluid velocity is higher, proppant grains start to roll or slide along the surface of settled proppant bank. If the fluid velocity is even higher such that the sum of drag and lift forces is greater than the submerged force (gravity plus buoyancy), proppant grains can bounce off the surface and go back into the flow stream.

In order to quantify the particle movement in relation to proppant bed and based on a range of experimental models, Shields (1936) defined a critical shear stress to determine when particles start to move from the bed. Specifically, the Shields number is defined as the ratio between shear and apparent weight on a single particle:

$$S = \frac{\tau_b}{(\rho_p - \rho_f) g d_p} \tag{24}$$

where τ_b is the shear stress acting on the top of the bank.

The average shear stress for a flow into a slot can be defined as (Biot and Medlin, 1985):

$$\tau_b = \frac{1}{8} c_f \rho_f v_f^2 \tag{25}$$

where c_f is a friction coefficient dependent on the Reynolds number *Re*.

Substituting Eq. (25) into Eq. (24) yields the fluid flow velocity to cause bed erosion (McClure, 2018):

$$v_f = \sqrt{\frac{S \cdot 8 (\rho_p - \rho_f) g d_p}{c_f \rho_f}} \tag{26}$$

McClure (2018) found that the bed transport begins at a Shields number between 0.03 and 0.06.

In the presence of a proppant bank, there are three widely acknowledged proppant transport modes: suspension, saltation and reptation (or creep), as shown in Fig. 4. The suspension usually occurs at the early stage of a mixture injected into the fracture. After that, the proppant bank starts to build due to continuous particle settling, which then leads to the saltation and reptation modes (McLennan et al., 2008). In terms of numerical simulation, the suspension process can be modelled by the approaches described in § 2.3. However, to model saltation and reptation, it is necessary to consider the micromechanical interactions between particles (Duran, 2000). As shown in Fig. 4, reptation refers to the mode of particles starting to roll or creep at the top of proppant bank after settling, and saltation refers to the jump of particles that were previously on the surface of the proppant bed. The creep movement is initiated by the shear stress, which is directly related to the fluid velocity. Therefore, reptation is sensitive with respect to the fluid velocity variation. In the saltation mode, particles go into the flow stream, travel downward and then land back to proppant bed. As particles bounce between flow stream and proppant bed in the saltation mode, it is also named as intermittent suspension. Concluded in (Wilcock and Crowe, 2003), a significant amount of particles travel close to the bed surface. Thus, depending on the mass of those particles and the transport momentum, when those particles land again from the jump, they can collide and kick other particles into the flow stream. Such complex behaviour can also happen with the next batch of lading particles.

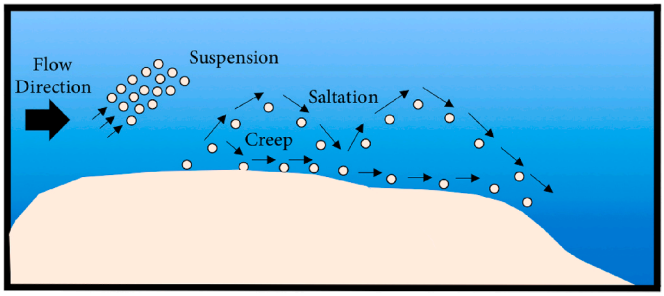

Fig. 4. Schematic for proppant transport mechanisms.

2.7. Types of proppants

Over the years, different types of proppants have been developed, tested and adopted by the petroleum industry in hydraulic fracturing treatment, and they are often classified as natural sand, ceramic and resin-coated proppants (Pangilinan et al., 2016). To date, sand remains as the most widely used proppant material by the industry (Liang et al., 2016). It should be noted that even though sand is a natural material, a series of production processes are still required to extract the material from deposits, crush, clean, dry and size before it can be used in hydraulic fracturing treatment.

Ceramic proppants are developed to overcome the pressure resistance barrier from the sand. There are vast base material options for producing ceramic proppants, such as bauxite, kaolin, magnesium silicate, and blends of bauxite and kaolin. Thus, the industry often further subdivide ceramic proppants into three categories: high-density (relative density 3.5 g/cm^3), intermediate-density (relative density 3.27 g/cm^3) and low density (relative density 2.55 ~ 2.71 g/cm^3) ceramic proppants. The strength of ceramic proppants typically increases with the density (Danso et al., 2020).

Resin-coated sand/ceramic proppants are developed to enhance the conductivity of traditional sand and ceramic grains, and they can be either pre-cured or cured in-situ. The main advantage (or purpose) of resin-coated proppants is to trap broken grains and connect individual grains to prevent flowback (Zoveidavianpoor and Gharibi, 2015). However, since the coating is made of polymers, the temperature can affect their mechanical response compared to inorganic proppants

(Liang et al., 2016).

Choosing the most effective proppant type depends largely on the geomechanical conditions of the reservoir, e.g. *in situ* stress, temperature and permeability (Ahamed et al., 2020). Moreover, the stress transferred from reservoir to proppant particles after releasing the fracturing fluid must be treated with caution to avoid proppant crushing, proppant embedment and fines generation, all of which could reduce the fracture width (Han and Wang, 2014). With respect to the proppant shape, traditionally it has been believed that the ideal proppant shape is spherical or nearly spherical, and non-angular as much as possible (Liang et al., 2016). However, different shapes of proppants other than conventional spherical shape have been developed in recent studies. Jia et al. (2019) suggested that rod-shaped proppants have been implemented in several countries with consistent success in increasing stimulation efficiency. Elongated rod-shaped proppant is believed to be a promising candidate to increase pack permeability and prevent mature screen-outs (Klyubin et al., 2015). Additionally, due to its geometry, flowback tend to be reduced (Mcdaniel et al., 2010). For numerical modelling, Osiptsov (2017) highlighted the importance of improving models to consider the effect of proppant crushing.

2.8. Leak-off, flowback, and tip screenout

Both the design target and the practical behaviour of proppant transport may be directly affected by the stage and status of hydraulic fracturing operation. One such example is the influence from leak-off, i.e. a fracturing fluid escaping to the surrounding reservoir rock. The outflow of fracturing fluid causes an increase of proppant concentration in the slurry, hence an increase of the slurry viscosity, which arguably increases the risk of forming a jammed area in the fracture. One of the most widely accepted model to quantify the effect of leak-off on the slurry flow is Carter's formula (Howard and Fast, 1957):

$$q_L = \frac{C_L}{\sqrt{t - t_0}} \tag{27}$$

where q_L is the flux of fracturing fluid that is leaking, t_0 the start time of the fracturing fluid escaping into the reservoir zone, and C_L the leak-off coefficient. The above relation is analytically obtained for a semi-infinite porous medium, and it only represents an overly simplified estimation in many practical situations, e.g. near the fracture tip.

Existing leak-off models usually consider 1D permeation orthogonal to the fracture surface, while the practical leak-off process is more complex. Wang et al. (2018a) considered leak off in a pressure-sensitive dual porosity medium, where the proppant distribution in the hydraulic fracture is determined by integrating a constitutive equation in the formulation. In a scenario of dual porosity, the results show a substantial increase in the amount of proppant carried into the hydraulic fracture. It is also found that decreasing the leak-off rate leads to a wider main fracture and delays the occurrence of proppant screenout.

Another stage in hydraulic fracturing that directly affects proppant transport is flowback. Flowback is the clean up stage before the hydrocarbon production, and it is governed by the fracture width, the hydrodynamic gradient and the closure stress of the system (Andrews and Kjorholt, 1998). Ideally, one would hope only the fracture fluid flows back so that proppant pack remains intact (Dogon and Golombok, 2016), but it is common to also have proppants coming out as well (McLennan et al., 2008), causing such unwanted consequences as fracture closing and tapering out near the wellbore. Dogon and Golombok (2016) highlighted how fracturing fluid must be selected carefully since it should display two conflicting rheological characteristics: high carrying capacity for the placement phase of proppants and low carrying capacity during the succeeding flowback phase. A viscoelastic fluid was tested in (Dogon and Golombok, 2016) and the authors suggested that flow-induced viscoelasticity can be used for proppant placement and flow back without the need to add modifying chemicals. However, chemicals are still being adopted by the industry, bringing the discussion about environmental issues.

Tip screenout is a technique commonly used to increase fracture conductivity, where the slurry is injected at high pressure and high proppant load close to the fracture tip (Economides and Nolte, 2000). However, in practice, pack formation from tip screenout sometimes occurs at a wrong time, ending up at an unwanted position (Chekhonin and Levonyan, 2012). A pack formation in an inconvenient location can lead to a bad proppant disposition, affecting the final fracture state (Dontsov and Peirce, 2015).

3. Proppant transport modelling

Proppant transport modelling is a critical part of hydraulic fracturing simulators, especially in commercial software for hydraulic fracturing design. The ability to accurately predict the proppant distribution throughout the hydraulic fracturing process is significant for the design and planning of a successful fracturing treatment. Characterized by the mixing of carrier fluid and proppant particles, the slurry flow can be investigated using multiphase flow simulation. Both Eulerian-Eulerian and Eulerian-Lagrangian schemes have been used for proppant transport modelling, and they are reviewed in § 3.1 and § 3.2, respectively.

3.1. Proppant transport modelling with Eulerian-Eulerian scheme

Using Eulerian-Eulerian scheme, fracturing fluid and proppant particles are treated as interpenetrating continua, and a volume in space can be occupied by both phases at the same time. Thus, the volume fraction, a continuous function of space and time, is introduced to represent how much space is occupied by each phase at any given time. For instance, in a two-phase solid-liquid mixture, there are two volume fractions, one for the solid phase and the other for the liquid phase, while all volume fractions add up to one. Both the fluid flow and particle movement are described by the evolution of corresponding volume fraction.

Compared to Eulerian-Lagrangian scheme, Eulerian-Eulerian scheme is often easier to implement and has a lower computational cost. Therefore, it has been extensively used for proppant transport modelling since the beginning of the development of hydraulic fracturing simulators. The governing equations are also easily coupled with the rock deformation and fracture propagation. There are two main types of Eulerian-Eulerian schemes suitable for proppant transport modelling: the mixture model and the two-fluid model. The mixture model only

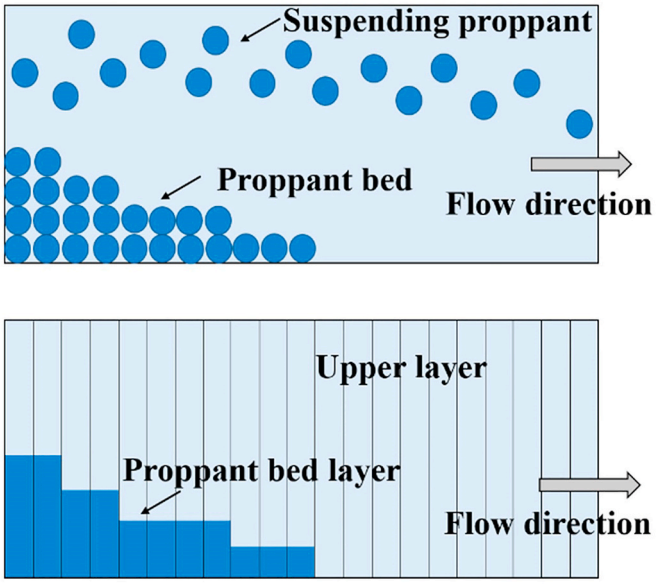

Fig. 5. Schematic for 2D proppant transport in a 1D flow (Hu et al., 2018b).

solves one set of Navier-Stokes equations (or the Poiseuille's law) for the slurry average, while the two fluid-model solves two sets of Navier-Stokes equations (or the Poiseuille's law) for the fluid and proppant phases separately.

3.1.1. Mixture model with 1D flow

In the hydraulic fracturing simulators that are based on PKN and cell-based P3D model (Perkins and Kern, 1961; Adachi et al., 2007), the fluid flow is simplified to be 1D along the direction of fracture propagation (see Fig. 5). However, with some simplifications and assumptions, the 2D proppant transport phenomena can still be simulated to a large extent, and they include the horizontal movement with fluid flow, the proppant settling in each vertical cell, and the formation of proppant bank.

Due to the cheap computation cost, the 2D proppant transport modelling in a 1D fluid flow has long been adopted in hydraulic fracturing modelling (Rahim and Holditch, 1992; Rahim et al., 1995; Smith et al., 1997). Hu et al. (2018b) proposed a new model for simulating the proppant transport in an idealized setup, i.e. a narrow channel formed by two parallel plates with a constant height. Taking this model as an example, the 2D proppant transport modelling in 1D fluid flow is briefly recapped here. As mentioned in § 2.2, the lubrication theory is applicable for fluid flows between narrow fracture surfaces, where the slurry velocity is expressed as

$$v = \frac{w^2}{12\mu}\frac{\partial p}{\partial x} \tag{28}$$

The slurry velocity increases as the proppant bed builds up. Considering the mass conservation, the slurry velocity (also the horizontal component of the particle velocity) is expressed as

$$v = v_{px} = \frac{H - H_{bed}}{H}\frac{w^2}{12\mu}\frac{\partial p}{\partial x} \tag{29}$$

where H and H_{bed} are the height of the fracture and the proppant bed, respectively. The height of proppant bed H_{bed} is determined by the rate of proppant bed build-up H_b and the rate of proppant bed wash-out H_w, which are related to the settling velocity and slurry velocity above the bed. In this model, the vertical component of the particle velocity equals to the settling velocity and is calculated by Eq. (14)

$$v_{py} = v_s \tag{30}$$

Given the particle velocity $\boldsymbol{v}_p$, the proppant concentration in the domain above the proppant bed is updated according to the continuity equation for the particle phase:

$$\frac{\partial(cw)}{\partial t} + \nabla\cdot\left(cw\boldsymbol{v}_p\right) = 0 \tag{31}$$

In each time step, Eqs. (29)–(31) are solved iteratively and then the height of proppant bed is updated according to the slurry velocity and setting velocity. Details of the algorithm can be found in (Hu et al., 2018b), which also compares the numerical results with experiments in the literature demonstrating good agreement.

Dontsov and Peirce (2015) developed a proppant transport model coupled with a P3D hydraulic fracturing model. Both the proppant settling and crack-tip screenout are accounted for. The numerical results show that the particles can reach the fracture tip even without leak-off. This is because the proppant is concentrated near the centre of the channel, and therefore gets transported faster than the fracturing fluid. When leak-off is considered, the proppant reaches the crack tip region notably faster and forms a plug. Once the plug is developed, only a small amount of fluid can penetrate the plug, which switches the fracture growth predominantly to the vertical direction.

This kind of model is also used in the hydraulic fracturing design software based on the PKN or P3D models, for example, the unconventional fracture model (UFM) in Kinetix Shale by Schlumberger Ltd.

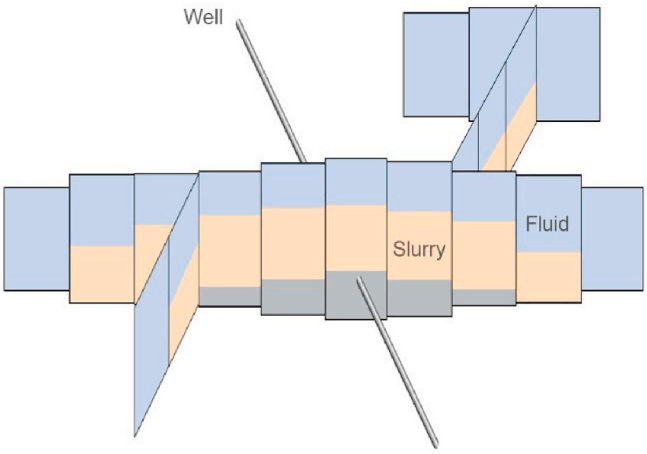

Fig. 6. A three-layer proppant transport model in UFM (Badessich et al., 2016).

(Weng et al., 2014). A schematic illustration for the proppant transport in a fracture network using UFM is shown in Fig. 6.

3.1.2. Mixture model with 2D flow

In the context of hydraulic fracturing, the slurry flows along a fracture (planar or non-planar) with very narrow width, which is governed by the Poiseuille's law in Eq. (5). The relationship between the slurry velocity $\boldsymbol{v}$ and the particle velocity $\boldsymbol{v}_p$ is expressed as (Adachi et al., 2007):

$$\boldsymbol{v}_p = \boldsymbol{v} - (1-c)\boldsymbol{v}_{slip} \tag{32}$$

where $\boldsymbol{v}_{slip}$ is the slip velocity between the particle and fluid, as discussed in § 2.3.

Once the particle velocity is determined, the proppant concentration over the fracture is updated through the continuity equation for the proppant phase using Eq. (31). The above governing equations Eqs. (4), (5), (31) and (32) describe the key physics behind proppant transport. The bed formation is naturally simulated since the settling velocity reduces to zero due to the significant increase of viscosity when the proppant concentration approaches to the packing limit (see § 2.5).

The 2D proppant transport model has a high efficiency and can be easily implemented, which makes it one of the most popular proppant transport models in hydraulic fracturing simulators since 1980s (Clifton and Wang, 1988; Ouyang et al., 1997; Adachi et al., 2007). Clifton and Wang (1988) coupled the proppant transport modelling with the dynamic propagation of hydraulic fracture in a PL3D model. The hindered proppant settling, wall effect, leak-off and temperature effects are all considered. It is found the high temperature can cause poor proppant distribution, due to the reduction of the fracturing fluid viscosity. A similar model was presented in (Adachi et al., 2007).

Roostaei et al. (2018) simulated the proppant transport in two simplified configurations: rectangular and elliptic fractures with constant fracture length, width and height. The effects of injection rate, proppant density and size, fluid viscosity on the proppant transport are investigated. In addition, the impact of convection and proppant settlement on the vertical motion of proppants is investigated. It concludes that the fluid viscosity has the strongest effect on the proppant settling while the proppant size and density only have modest effect under practical conditions.

3.1.3. Two-fluid model with 2D flow

Another popular Eulerian-Eulerian scheme for proppant transport modelling is the two-fluid model, which models the proppant transport with two sets of Navier-Stokes equations coupled through an inter-phase force (Boronin and Osiptsov, 2010, 2014; Gong et al., 2020): one set of the equations is for the fracturing fluid phase and the other for the

proppant phase. When the fluid velocity in the direction of fracture width is assumed to be zero, the lubrication theory is applicable (Mobbs and Hammond, 2001; Dontsov and Peirce, 2014a; Shiozawa and McClure, 2016).

Based on the lubrication theory, Pearson (1994) presented a proppant transport model with two sets of governing equations for the fluid and proppant respectively. A set of two-dimensional variables are obtained by integration of the standard three dimensional equations across the fracture width and subsequently they are used to describe the suspension transport inside the fracture space. Later, Hammond (1995) and Mobbs and Hammond (2001) proposed explicit mass flux relations for the governing equations from (Pearson, 1994).

Proppant transport has also been modelled by using empirical constitutive relations (Dontsov and Peirce, 2014a), where shear stress and particle pressure are expressed as functions of proppant concentration (Boyer et al., 2011). An advantage of such approach is the ability to handle the transition from Poiseulle flow to Darcy flow when proppant concentration increases. Later, the same model was applied to a complete hydraulic fracturing system (Dontsov and Peirce, 2015), which considers two classic fracture propagation models with the leak-off effect.

The proppant transport model developed by Dontsov and Peirce (2014a) was extended by Shiozawa and McClure (2016) to consider the fracture closure after injection stops, the vertical gravity-driven motion of proppant particles, and the tip screenout in a 3D hydraulic fracture. Their study concludes that an extremely low permeability of the matrix formation might cause poor proppant distribution, once proppants tend to settle due to gravity before the fracture closure.

3.2. Eulerian-Lagrangian scheme

Using the Eulerian-Lagrangian approach, the fluid phase is treated as a continuum solved in Eulerian grids, while the dispersed phase is treated as discrete particles described by Newton's law. More mechanisms of proppants movement can be considered by using the Eulerian-Lagrangian scheme, since it simulates the particle movement more accurately. Two different Eulerian-Lagrangian schemes have been applied in proppant transport modelling: Computational Fluid Dynamics-Discrete Element Method (CFD-DEM) and Multiphase Particle-in-Cell Method (MP-PIC). In the framework of CFD-DEM, the proppant particles are individually simulated by DEM, while a group of particles with the same properties (named parcel) are tracked together in the MP-PIC model. The fundamentals of these two Eulerian-Lagrangian models and their applications in proppant transport modelling are reviewed in the following subsections.

3.2.1. CFD-DEM

For proppant transport modelling, the coupled approach of CFD-DEM has received increasing attention (Baldini et al., 2018; Kou et al., 2018; Suri et al., 2019). As a numerical methodology to solve a group of interactive moving particles, DEM has been used in a variety of applications, ranging from crushable soil (Cheng et al., 2003) and rock cutting (Onate and Rojek, 2004) to blood flow (Mountrakis et al., 2014). The CFD-DEM simulation has been used to investigate fluid-solid multiphase flow, and can also be applied to model proppant transport during hydraulic fracturing. The DEM typically uses 2D circular discs (or 3D spheres) to represent discrete particles, which are usually treated as rigid bodies constantly interacting with each other through collision.

The fluid is still governed by the Navier-Stokes equations. The particle acceleration is computed by the law of motion

$$\frac{\partial \boldsymbol{v}_p}{\partial t} = \frac{\boldsymbol{g}(\rho_p - \rho_f)}{\rho_p} + \boldsymbol{F}_{drag} + \boldsymbol{F}_{add} \tag{33}$$

where $\boldsymbol{F}_{add}$ is an additional acceleration term (force per unit particle mass) to account for virtual mass due to the reference-frame rotation and Brownian force, $\boldsymbol{F}_{drag}$ is the drag force term per unit of particle mass relevant to the relative or slip velocity and can be calculated with different models (Tsuo and Gidaspow, 1990; Suri et al., 2020b; Lu et al., 2020). The acceleration is assumed to be constant during the present time-step. A numerical integration then determines the position of each particle for the following time-step and the cycle repeats, propagating and transferring energy from particle to particle.

The interaction between particles is computed by using a contact model based on the small overlap between particles. As shown in Fig. 7, the necessary condition of two particles being in contact is:

$$d_{ij} \leq r_i + r_j \tag{34}$$

where d_{ij} is the distance between particle i and j from centre to centre, and r_i and r_j are the particle radii.

CFD-DEM has been applied in proppant transport modelling in simplified configurations of an idealized rectangular fracture geometry with constant width to investigate the relevant mechanisms. Zhang et al. (2017b) applied CFD-DEM in simulating the proppant transport in

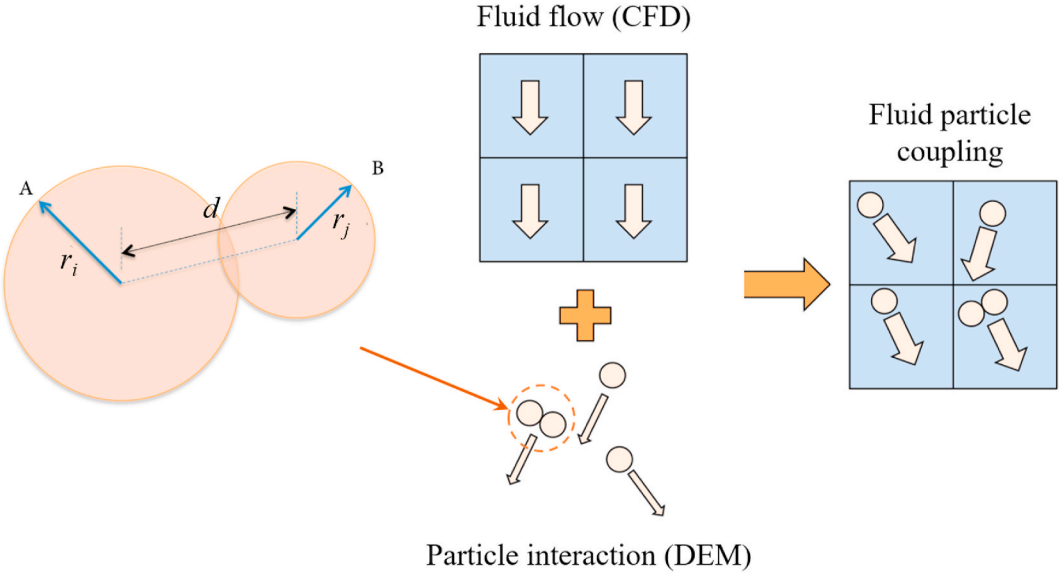

Fig. 7. Schematic for CFD-DEM coupling.

horizontal wells. The commercially-available Particle Flow Code PFC2D with a coupled CFD-DEM approach is used. The fluid flow is modelled based on a finite difference solution of the modified Navier-Stokes equations in a regular finite difference grid, while DEM is used to simulate particles including the particle-particle and particle-wall interactions. The same model was also applied in simulating the transport and placement of multi-sized proppants in a hydraulic fracture in vertical wells (Zhang et al., 2017a). A sensitivity study of fluid viscosity, injection rate, and perforation positions is conducted. Suri et al. (2020b) performed a parametric study to investigate the effect of variation in proppant size, fluid viscosity and fracture width on the proppant transport. It is suggested that smaller proppants can be injected early, followed by larger proppants to maintain high propping efficiency. Baldini et al. (2018) investigated the effect of the position of injection point and proppant injection strategies on the proppant distribution. An injection point placed close to the bottom of the cell leads to a dune close to the injection points, and an injection point at the middle or at the top of the cell leads to a rather flat dune. Injecting different proppant types in different orders yields distinctive proppant distributions. Through CFD-DEM simulation, Lu et al. (2020) concluded that high-viscosity fracturing fluid and low-density proppant should be pumped first to increase the distance of proppant placement and increase the effective fracture stimulation area. Thereafter, low-viscosity fracturing fluid and high-density proppant are pumped to form fractures with high conductivity in the near-well zone, effectively improving the condition of the near-well zone.

Some other variations of the simplified configurations have been designed to investigate specific mechanisms. Kou et al. (2018) investigated the proppant transport in vertical and inclined hydraulic fractures with CFD-DEM. The DEM simulation is performed through an open source C++ simulator parallelized with MPI and CUDA. Using the parallelized code and high performance computing facilities, large-scale simulations involving realistic fluid injection velocities much larger than that in laboratory experiments are conducted. It is found that proppants settle slower in inclined fractures. Wang et al. (2019) computed the proppant transport in idealized fracture networks considering the aperture difference, the orientation of branch fractures and the leak-off in fracture tips. The numerical simulations show that the small angle between main hydraulic fracture and branches and the big branch aperture are advantageous to the proppant particles getting into the branch.

An upscaling CFD-DEM was developed by Zeng et al. (2016) and was applied in modelling the proppant transport in a PKN hydraulic fracturing model. As modelling every individual particle is time consuming, the representative particle method is therefore adopted. It is concluded that viscous fluid tends to carry the proppant further, and also the lighter the proppant the further it is transported.

Blyton et al. (2015, 2018) incorporated the CFD-DEM model with a PL3D hydraulic fracturing model to simulate the proppant transport along with dynamic fracture propagation. The open source CFD library OpenFoam (Open Source Field Operation and Manipulation) is used to solve the fluid flow field. It is found that the average proppant phase velocity is generally lower than the average fluid phase velocity with a reduction in velocity linearly proportional to the volumetric concentration of proppant. The average proppant settling velocity may be larger or smaller than that predicted by Stokes' law, with additional dependencies on proppant diameter to slot width, concentration and Reynold's number. The combination of slower proppant transport and potentially faster settling leads to a marked reduction in propped fracture lengths, compared to the predictions made with simplified proppant transport assumptions commonly used in industry.

CFD-DEM has also been applied in modelling proppant transport in multiple perforation clusters by incorporating with a hydraulic fracture model that supports simultaneous propagation of multiple planar fractures (Wu et al., 2017). Several observations are made from the numerical results: (1) the proppant concentration in the slurry increases as the slurry flows from the heel side to the toe side; (2) the slurry concentration can be several times higher than the injected proppant concentration at the toe cluster; (3) the stress shadow effect from fractures of previous stage suppresses fracture propagation from the toe-side clusters, which promotes a heel biased fluid distribution.

Tomac and Gutierrez (2015) improved the CFD-DEM interaction by incorporating fluid lubrication with particle-particle collision, and studied the fluid lubrication as an agglomeration mechanism. The study investigates whether the existing proppant relations are useful for narrow fracture zones and under which conditions they could be acceptable. It is found that the existing relationships are not appropriate for fracture zones containing particle volumetric greater than 0.2 and the fluid viscosity also could not be higher than 0.005 Pa·s. CFD-DEM has also been applied in simulating the permeability of proppant pack with different types of proppant particles (Kulkarni and Ochoa, 2012, 2017). Basu et al. (2014); Suri et al. (2020b) compared the CFD-DEM and the two-fluid models for proppant transport simulation with the same configurations, and several observations are made in relation to the simulation efficiency and accuracy.

3.2.2. MP-PIC

MP-PIC (Tsai et al., 2012; Zeng et al., 2019; Siddhamshetty et al., 2020) is another kind of Eulerian-Lagrangian model for modelling proppant transport. The main difference between the CFD-DEM model and the MP-PIC model is how to deal with the dispersed phase (i.e. proppant particles) (Siddhamshetty et al., 2020). In CFD-DEM models, each individual particle is individually simulated such that the velocity and position of every particle are calculated by integrating the forces acting on them over time. The CFD-DEM model captures the proppant transport at relatively small scales, but is difficult to be applied in field-scale simulations due to the extremely high computational cost. In MP-PIC models, the dispersed phase is approximated by many parcels, and each parcel contains a group of proppant particles (see Fig. 8). Because of these characteristics, MP-PIC models are able to capture the important features of proppant transport in field-scale geometries at a greatly reduced computational cost.

The dynamics of the particle phase in the MP-PIC method are described by a particle probability distribution function $\varphi(\boldsymbol{x}_p, \boldsymbol{v}_p, \rho_p, V_p, t)$ where $\boldsymbol{x}_p$, $\boldsymbol{v}_p$, ρ_p, and V_p are the particle position, velocity, density, and volume, respectively. The time evolution of function φ is obtained by

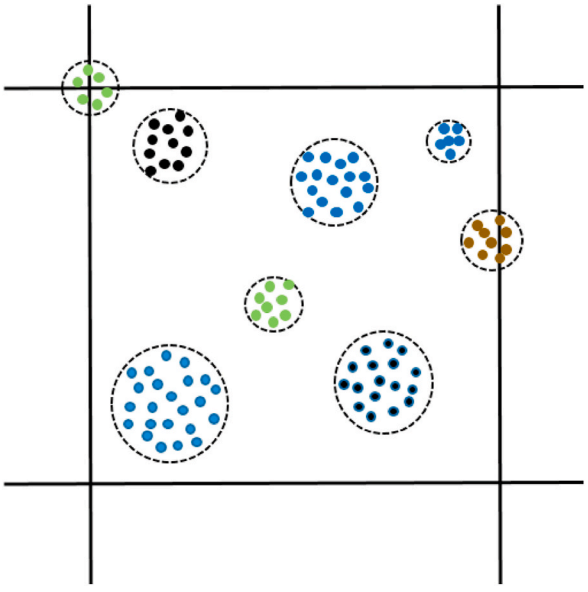

Fig. 8. Schematic for parcels with different sizes in the MP-PIC model (Siddhamshetty et al., 2020).

solving the following equation (Zeng et al., 2019; Siddhamshetty et al., 2020):

$$\frac{\partial \varphi}{\partial t} + \nabla_{x_p} \cdot (\varphi \boldsymbol{v}_p) + \nabla_{v_p} \cdot (\varphi \boldsymbol{A}) = 0 \tag{35}$$

$$\boldsymbol{A} = \frac{d\boldsymbol{v}_p}{dt} = D_p(\boldsymbol{v}_f - \boldsymbol{v}_p) - \frac{1}{\rho_p}\nabla p + \boldsymbol{g} - \frac{1}{c\rho_p}\nabla \tau_p \tag{36}$$

where ∇_{x_p} and ∇_{v_p} are the spatial and velocity divergence operator, $\boldsymbol{A}$ is the proppant parcel acceleration, τ_p is the inter-particle stress, D_p is the drag coefficient expressed as (Siddhamshetty et al., 2020)

$$D_p = C_d \frac{3\rho_f |\boldsymbol{v}_f - \boldsymbol{v}_p|}{8\rho_p r} \tag{37}$$

where

$$C_d = \begin{cases} \dfrac{24\left(1 + 0.15Re_p^{0.687}\right)}{Re_p}\varphi^{-2.65}, Re_p < 1000 \\ 0.44\varphi^{-2.65}, Re_p > 1000 \end{cases} \tag{38}$$

Although the MP-PIC approach has been widely adopted in other particulate systems (e.g. (Gupta et al., 2021)), its application to proppant transport modelling is still limited. The capacity of MP-PIC in simulating proppant transport was first demonstrated by Tsai et al. (2012) in a 3D highly idealized fracture geometry. Zeng et al. (2019) simulated the proppant transport in large-scale propagating fractures by coupling the MP-PIC for proppant transport modelling and PKN model for fracture propagation. The Lagrangian feature of the MP-PIC model supports simulating the transport of proppants with multi-densities and/or multi-sizes. It is found that MP-PIC performs similar to the CFD-DEM but has a lower computational cost and reaches a good balance in the trade-off of computational cost and accuracy. A 3D MP-PIC model was applied in simulating the multi-size proppant transport in a field-scale geometry (Siddhamshetty et al., 2020). The study shows that pumping schedules significantly affects props fracture surface area and average fracture conductivity, thereby influencing shale gas production.

3.3. Summary of proppant transport models

The numerical models in Eulerian-Eulerian scheme (§ 3.1) and the Eulerian-Lagrangian scheme (§ 3.2) are summarized and compared in Table 1. The Eulerian-Eulerian scheme has been extensively used in proppant transport modelling in commercial software for hydraulic fracturing design, while till now the Eulerian-Lagrangian scheme has mostly been used in academic studies with few applications in modelling field-scale proppant transport. Among different Eulerian-Eulerian schemes, the mixture model is most popular thanks to its high efficiency, good stability and easy implementation. The two-fluid model has a higher accuracy than the mixture model. However, neither of them can capture the high-resolution interaction between particles, which is the main advantage of the Eulerian-Lagrangian schemes. A common drawback of the Eulerian-Lagrangian approach is the high computational cost. Also, when the particle deposition approaches the packing limit, it is very difficult to maintain a stable simulation. The recent advances show the possibility of simulating the field-scale proppant transport with the Eulerian-Lagrangian scheme (Zeng et al., 2019).

4. Conclusions and recommendations for future work

4.1. Conclusions

Proppant injection after opening a hydraulic fracture is crucial to increase formation permeability and thereby improve production in unconventional reservoirs. Thus, for both planning and operational purposes, it is important to understand the proppant transport inside hydraulic fractures as accurately as possible. Due to the technical difficulties and high cost associated with *in situ* measurement and real-time monitoring, computer simulation is recognized as the most promising approach to provide a reliable and detailed understanding for proppant transport. Hence, to promote the research progress, we present a state-of-the-art review on proppant transport modelling, and to our knowledge this is the first dedicated review on the topic. Some main remarks on the literature are summarized below.

The Eulerian-Eulerian scheme is widely used for the simulation of proppant transport, especially when coupled with fracture propagation. The Eulerian-Eulerian scheme has a higher efficiency and is easier to implement than the Eulerian-Lagrangian scheme. The mixture model solves a single Navier-Stokes equation (or Poiseuille's law) with respect to the slurry average and the computational cost is essentially at the same level as the single phase fluid flow. Both horizontal movement and vertical settling can be modelled with the mixture model no matter the fluid flow in the hydraulic fracturing model is 1D or 2D. The mixture model for 1D flow has been coupled with the PKN and P3D hydraulic fracturing models while the mixture model for 2D flow has been incorporated with the PL3D model. Another type of the Eulerian-

Table 1
Summary of numerical models for proppant transport.

Scheme	Model	Fluid-particle interaction	Particle-particle interaction & packing	Advantages	Disadvantages	Applications in different fracture models
Eu–Eu	Mixture model 1D flow	One way coupled	Equilibrium proppant bank height	High efficiency and easy implementation	Inaccuracy and lack of physical mechanisms; Applicability to only low load of particles	Simplified model* (Hu et al., 2018b), PKN model (Kong et al., 2015; Wang et al., 2018b), P3D model (Rahim and Holditch, 1992)
	Mixture model 2D flow	Two way coupled	Modified settling velocity	High efficiency and easy implementation	Inaccuracy and lack of physical mechanisms; Applicability to only low load of particles	Simplified model (Roostaei et al., 2018), PL3D mode (Adachi et al., 2007; Clifton and Wang, 1988)
	Two-fluid model 2D flow	Two way coupled	Modified settling velocity	Higher accuracy than mixture model	Higher computational cost and lower computational stability	Simplified model (Boronin and Osiptsov, 2014) DFN (Shiozawa and McClure, 2016)
Eu–La	CFD-DEM 2D flow	Two way coupled	Fully resolved	Highest accuracy in capturing fluid-particle and particle-particle interaction; Applicability to case of high volume fraction of particle	Very high computational cost for field-scale problems; Difficulty in coupling with dynamic fracture propagation and complex fracture geometry	Simplified model (Wang et al., 2019), PL3D model (Blyton et al., 2015, 2018)
	MP-PIC 2D flow	Two way coupled	Particle stress model	Good balance on time cost and accuracy	Difficulty in coupling with dynamic fracture propagation and complex fracture geometry	Simplified model (Siddhamshetty et al., 2020) PKN model (Zeng et al., 2019)

Note: the simplified model* has an idealized rectangular fracture geometry with constant width.

Eulerian scheme is the two-fluid model which solves two sets of Navier-Stokes equations (or Poiseuille's law) for the fracturing fluid and proppant particles respectively. It has a higher computational cost but also higher accuracy than the mixture model. The two-fluid model has been applied in modelling the proppant transport in the simplified model and the DFN model.

The Eulerian-Lagrangian scheme is an emerging approach for modelling proppant transport in recent years. It treats the fracturing fluid as a continuum governed by the Navier-Stokes equations (or Poiseuille's law) and the proppants as discrete particles following Newton's law. The two Eulerian-Lagrangian schemes applied in proppant transport modelling are CFD-DEM and MP-PIC. The CFD-DEM model tracks individual particles while the MP-PIC tracks a parcel of particles with the same property. Therefore, the MP-PIC model has a lower computational cost than the CFD-DEM model but both of the two are much more expensive than the Eulerian-Eulerian approaches. The high computational cost of the Eulerian-Lagrangian limits its application in field-scale modelling of proppant transport. The advantage of the Eulerian-Lagrangian scheme is also obvious: it provides the highest possible modelling resolution for the behaviour of proppant particles. With the increase of computing power, the coupling between the Eulerian-Lagrangian scheme for proppant transport and the simulation of hydraulic fracture propagation has emerged.

4.2. Recommendations for future work

As discussed above, traditional numerical approaches for simulation of multiphase flow as well as other specifically designed simplified models have been applied in proppant transport modelling. Despite the extensive research works and the great success, further research in the following directions are still needed in order to address the drawbacks and limitations in current models.

- As demonstrated in literature (Blyton et al., 2015), the widely used simplified numerical models for proppant transport in hydraulic fracturing are often found to over-predict propped or effective fracture lengths. The further development and application of Eulerian-Lagrangian models (e.g. MP-PIC) is encouraging (Zeng et al., 2019). However, the efficiency of the program still needs to be improved to target field-scale simulation with realistic fracture geometry.
- The sensitivity study and design of injection strategy needs to be conducted through proppant transport modelling coupled with dynamic fracture propagation instead of idealized configurations with constant height, width and length.
- The proppant transport modelling in current hydraulic fracturing simulators mostly consider the basic physical processes such as convection and settling, but is not comprehensive enough to capture all key mechanisms relevant to proppant transport.
- Subsurface detection technique for tracking proppants (Palisch et al., 2017) can be used for calibrating the proppant transport modelling in field problems.

Declaration of competing interest

The authors declare that they have no known competing financial interests or personal relationships that could have appeared to influence the work reported in this paper.

Acknowledgements

The authors would like to thank the financial support from Brazilian National Council for Scientific and Technological Development (CNPq), the Royal Academy of Engineering, and the National Research Network of Wales Government.

References

Adachi, J., Siebrits, E., Peirce, A., Desroches, J., 2007. Computer simulation of hydraulic fractures. Int. J. Rock Mech. Min. Sci. 44 (5), 739–757.
Ahamed, M.A.A., Perera, M.S.A., Black, J.R., Matthai, S.K., Ranjith, P.G., Dong-yin, L., Sampath, K.H.S.M., 2020. Investigating the proppant damage mechanisms expected in a propped coal fracture and its effect on fracture flow. J. Petrol. Sci. Eng. 108170.
Al-Muntasheri, G.A., 2014. A critical review of hydraulic fracturing fluids over the last decade. In: *SPE Western North American and Rocky Mountain Joint Meeting*, Volume All Days. SPE-169552-MS.
Andrews, J., Kjorholt, H., 1998. Rock mechanical principles help to predict proppant flowback from hydraulic fractures. In: SPE/ISRM Rock Mechanics in Petroleum Engineering. Society of Petroleum Engineers, pp. 381–390.
Andrews, M.J., O'Rourke, P.J., 1996. The multiphase particle-in-cell (MP-PIC) method for dense particulate flows. Int. J. Multiphas. Flow 22 (2), 379–402.
Ansys, 2009. Ansys Fluent 12.0. Ansys Inc.
Austin, P.R., Nogami, H., Yagi, J.-i., 1997. A mathematical model of four phase motion and heat transfer in the Blast Furnace. ISIJ Int. 37 (5), 458–467.
Babcock, R.E., Prokop, C.L., Kehle, R.O., 1967. Distribution of Propping Agent in Vertical Fractures. Drilling and Production Practice.
Badessich, M., Hryb, D., Suarez, M., Mosse, L., Palermo, N., Pichon, S., Reynolds, L., 2016. Vaca muerta shale-taming a giant. Oilfield Rev. 28 (1), 14.
Baldini, M., Carlevaro, C.M., Pugnaloni, L.A., Sánchez, M., 2018. Numerical simulation of proppant transport in a planar fracture. a study of perforation placement and injection strategy. Int. J. Multiphas. Flow 109, 207–218.
Barati, R., Liang, J.-T., 2014. A review of fracturing fluid systems used for hydraulic fracturing of oil and gas wells. J. Appl. Polym. Sci. 131 (16) n/a–n/a.
Barree, R., Conway, M., 1995. Experimental and numerical modeling of convective proppant transport. J. Petrol. Technol. 47 (3), 216–222, 0.
Basu, D., Das, K., Smart, K., Ofoegbu, G., 2014. Comparison of eulerian-granular and discrete element models for simulation of proppant flows in fractured reservoirs. In: ASME 2015 International Mechanical Engineering Congress and Exposition, 7B. Fluids Engineering Systems and Technologies. V07BT09A012.
Batchelor, G.K., 2000. An Introduction to Fluid Dynamics. Cambridge university press.
Belyadi, H., Fathi, E., Belyadi, F., 2017. Hydraulic Fracturing in Unconventional Reservoirs. Gulf Professional Publishing, Boston.
Biot, M., Medlin, W., 1985. Theory of Sand Transport in Thin Fluids. SPE Annual Technical Conference and Exhibition.
Blyton, C.A., Gala, D.P., Sharma, M.M., 2018. A study of proppant transport with fluid flow in a hydraulic fracture. SPE Drill. Complet. 33 (4), 307–323, 0.
Blyton, C.A.J., Gala, D.P., Sharma, M.M., 2015. A Comprehensive Study of Proppant Transport in a Hydraulic Fracture, pp. 28–30. September.
Boronin, S.A., Osiptsov, A.A., 2010. Two-continua model of suspension flow in a hydraulic fracture. Dokl. Phys. 55 (4), 199–202.
Boronin, S.A., Osiptsov, A.A., 2014. Effects of particle migration on suspension flow in a hydraulic fracture. Fluid Dynam. 49 (2), 208–221.
Boyer, F., Guazzelli, E., Pouliquen, O., 2011. Unifying suspension and granular rheology. Phys. Rev. Lett. 107 (18), 188301.
Carter, B.J., Desroches, J., Ingraffea, A.R., Wawrzynek, P.A., 2000. Simulating fully 3D hydraulic fracturing. In: Zaman, M., Booker, J., Gioda, G. (Eds.), Modelling in Geomechanics. Wiley, Hoboken, pp. 526–556 (chapter 21).
Chang, O., Kinzel, M., Dilmore, R., Wang, J.Y., 2018. Physics of proppant transport through hydraulic fracture network. J. Energy Resour. Technol. 140 (3).
Chang, O.C.-y., 2014. Modeling of Proppant Transport through Hydraulic Fracture Network. PhD Thesis. The Pennsylvania State University.
Chekhonin, E., Levonyan, K., 2012. Hydraulic fracture propagation in highly permeable formations, with applications to tip screenout. Int. J. Rock Mech. Min. Sci. 50, 19–28.
Chen, B., Barron, A.R., Owen, D., Li, C., 2018a. Propagation of a plane strain hydraulic fracture with a fluid lag in permeable rock. J. Appl. Mech. 85 (9), 091003–091003–10.
Chen, B., Cen, S., Barron, A.R., Owen, D., Li, C., 2018b. Numerical investigation of the fluid lag during hydraulic fracturing. Eng. Comput. 35 (5), 2050–2077.
Chen, B., Sun, Y., Barboza, B.R., Barron, A.R., Li, C., 2020. Phase-field simulation of hydraulic fracturing with a revised fluid model and hybrid solver. Eng. Fract. Mech. 229, 106928.
Cheng, Y.P., Nakata, Y., Bolton, M.D., 2003. Discrete element simulation of crushable soil. Geotechnique 53 (7), 633–641.
Clark, P.E., 2006. Transport of proppant in hydraulic fractures. In: SPE Annual Technical Conference and Exhibition. Society of Petroleum Engineers, p. 103167.
Clark, P.E., Quadir, J.A., 1981. Prop transport in hydraulic fractures: a critical review of particle settling velocity equations. In: SPE/DOE Low Permeability Gas Reservoirs Symposium volume All Days, SPE-9866-MS.
Cleary, M.P., Amaury Fonseca, J., 1992. Proppant convection and encapsulation in hydraulic fracturing: practical implications of computer and laboratory simulations. SPE Annual Technical Conference and Exhibition.
Cleary, M.P., Wright, C.A., Wright, T.B., 1991. Experimental and modeling evidence for major changes in hydraulic fracturing design and field procedures. SPE Gas Technol. Symp.
Clifton, R.J., Wang, J.J., 1988. Multiple Fluids, Proppant Transport, and Thermal Effects in Three-Dimensional Simulation of Hydraulic Fracturing. Society of Petroleum Engineers volume SPE-18198-MS.
Crowe, C.T., Schwarzkopf, J.D., Sommerfeld, M., Tsuji, Y., 2012. Multiphase Flows with Droplets and Particles, 2 edition. CRC Press.

Danso, D.K., Negash, B.M., Ahmed, T.Y., Yekeen, N., Arbi, T., Ganat, O., 2020. Recent advances on multifunctional proppant technology and icreased well output with micro and nano proppants. J. Petrol. Sci. Eng. 108026.
Detournay, E., 2016. Mechanics of hydraulic fractures. Annu. Rev. Fluid Mech. 48 (1), 311–339.
Dogon, D., Golombok, M., 2016. Self-regulating solutions for proppant transport. Chem. Eng. Sci. 148, 219–228.
Dontsov, E., Peirce, A., 2015. Proppant transport in hydraulic fracturing: crack tip screen-out in kgd and p3d models. Int. J. Solid Struct. 63, 206–218.
Dontsov, E.V., Peirce, A.P., 2014a. Slurry flow, gravitational settling and a proppant transport model for hydraulic fractures. J. Fluid Mech. 760, 567–590.
Dontsov, E.V., Peirce, A.P., 2014b. The effect of proppant size on hydraulic fracturing by a slurry. In: 48th US Rock Mechanics/Geomechanics Symposium. American Rock Mechanics Association, Minneapolis.
Duran, J., 2000. Sands, Powders and Grains - an Introduction to the Physics of Granular Materials, first ed. Springer Science+Business Media, New York.
Economides, M.J., Nolte, K.G., 2000. Reservoir Stimulation, 3 edition. John Wiley & Sons Ltd.
Einstein, A., 1905. On the motion of small particles suspended in a stationary liquid, as required by the molecular kinetic theory of heat. Ann. Phys. 322, 549–560.
Eskin, D., Miller, M.J., 2008. A model of non-Newtonian slurry flow in a fracture. Powder Technol. 182 (2), 313–322.
Fink, J.K., 2012. Chapter 17 - fracturing fluids. In: Fink, J.K. (Ed.), Petroleum Engineer's Guide to Oil Field Chemicals and Fluids. Gulf Professional Publishing, Boston, pp. 519–583.
Fink, J.K., 2013. Chapter 18 - proppants. In: Fink, J.K. (Ed.), Hydraulic Fracturing Chemicals and Fluids Technology. Gulf Professional Publishing, pp. 205–216.
Frankel, N., Acrivos, A., 1967. On the viscosity of a concentrated suspension of solid spheres. Chem. Eng. Sci. 22 (6), 847–853.
Gadde, P., Yajun, L., Jay, N., Roger, B., Sharma, M., 2004. Modeling proppant settling in water-fracs. Proceed. SPE Ann. Tech. Conf. Exhibit.
Gillies, R., Hill, K., McKibben, M., Shook, C., 1999. Solids transport by laminar Newtonian flows. Powder Technol. 104 (3), 269–277.
Gong, Y., Mehana, M., El-Monier, I., Viswanathan, H., 2020. Proppant placement in complex fracture geometries: a computational fluid dynamics study. J. Nat. Gas Sci. Eng. 79, 103295.
Gupta, S., Choudhary, S., Kumar, S., De, S., 2021. Large eddy simulation of biomass gasification in a bubbling fluidized bed based on the multiphase particle-in-cell method. Renew. Energy 163, 1455–1466.
Hammond, P., 1995. Settling and slumping in a Newtonian slurry, and implications for proppant placement during hydraulic fracturing of gas wells. Chem. Eng. Sci. 50 (20), 3247–3260.
Han, J., Wang, J.Y., 2014. Fracture conductivity decrease due to proppant deformation and crushing , a parametrical study. In: SPE Eastern Regional Meeting. Charleston.
Howard, G., Fast, C.R., 1957. Optimum fluid characteristics for fracture extension. In: Proceedings of the American Petroleum Institute, pp. 261–270.
Hu, X., Wu, K., Li, G., Tang, J., Shen, Z., 2018a. Effect of proppant addition schedule on the proppant distribution in a straight fracture for slickwater treatment. J. Petrol. Sci. Eng. 167, 110–119.
Hu, X., Wu, K., Song, X., Yu, W., Tang, J., Li, G., Shen, Z., 2018b. A new model for simulating particle transport in a low-viscosity fluid for fluid-driven fracturing. AIChE J. 64 (9), 3542–3552.
Huang, H., Babadagli, T., Andy, H., Develi, K., Wei, G., 2019. Journal of Petroleum Science and Engineering Effect of injection parameters on proppant transport in rough vertical fractures : an experimental analysis on visual models. J. Petrol. Sci. Eng. 180 (May), 380–395.
Hubbert, M., Willis, D., 1957. Mechanics of hydraulic fracturing. In: Petroleum Branch Fall Meeting, pp. 239–257 (Los Angeles. AIME).
Huitt, J.L., 1956. Fluid flow in simulated fractures. AIChE J. 2 (2), 259–264.
Jia, L., Li, K., Zhou, J., Yan, Z., Wan, F., Kaita, M., 2019. A mathematical model for calculating rod-shaped proppant conductivity under the combined e ff ect of compaction and embedment. J. Petrol. Sci. Eng. 180 (May), 11–21.
Kern, L., Perkins, T., Wyant, R., 1959. The mechanics of sand movement in fracturing. J. Petrol. Technol. 11 (7), 55–57, 0.
Klyubin, A., Konchenko, A., Parkhonyuk, S., Pavlova, S., Sitdikov, D., 2015. A new approach to improve fracturing in mature reservoirs , case study. In: SPE European Formation Damage Conference and Exhibition, Budapest.
Kong, B., Fathi, E., Ameri, S., 2015. Coupled 3-d numerical simulation of proppant distribution and hydraulic fracturing performance optimization in marcellus shale reservoirs. Int. J. Coal Geol. 147–148, 35–45.
Kou, R., Moridis, G.J., Blasingame, T.A., 2018. Analysis and modeling of proppant transport in inclined hydraulic fractures. In: SPE Hydraulic Fracturing Technology Conference and Exhibition volume Day 1 Tue, January 23, 2018, D011S002R001.
Kulkarni, M.C., Ochoa, O.O., 2012. Mechanics of light weight proppants: a discrete approach. Compos. Sci. Technol. 72 (8), 879–885.
Kulkarni, M.C., Ochoa, O.O., 2017. Creating novel granular mixtures as proppants: insights to shape, size, and material considerations. Mech. Adv. Mater. Struct. 24 (7), 605–614.
Lavrov, A., 2017. Coupling in hydraulic fracturing simulation. In: Shojaei, A.K., Shao, J. (Eds.), Porous Rock Fracture Mechanics. Woodhead Publishing, pp. 47–62.
Liang, F., Sayed, M., Al-Muntasheri, G.A., Chang, F.F., Li, L., 2016. A comprehensive review on proppant technologies. Petroleum 2 (1), 26–39.
Liu, Y., Gadde, P.B., Sharma, M.M., 2007. Proppant placement using reverse-hybrid fracs. SPE Prod. Oper. 22 (3), 15–17, 0.
Liu, Y., Sharma, M.M., Texas, U., 2005. Effect of Fracture Width and Fluid Rheology on Proppant Settling and Retardation : an Experimental Study. Spe, (SPE 96208):1 – 12.
Lu, C., Ma, L., Li, Z., Huang, F., Huang, C., Yuan, H., Tang, Z., Guo, J., 2020. A novel hydraulic fracturing method based on the coupled cfd-dem numerical simulation study. Appl. Sci. 10 (9), 3027.
Mack, M., Sun, J., Khadilkar, C., 2014. Quantifying proppant transport in thin fluids: theory and experiments. In: SPE Hydraulic Fracturing Technology Conference. Society of Petroleum Engineers.
McClure, M., 2018. Bed load proppant transport during slickwater hydraulic fracturing: insights from comparisons between published laboratory data and correlations for sediment and pipeline slurry transport. J. Petrol. Sci. Eng. 161 (May 2016), 599–610.
Mcdaniel, G., Corporation, A., Abbott, J., Mueller, F., Mokhtar, A., Pavlova, S., Nevvonen, O., Parias, T., Alary, J.A., 2010. Changing the shape of fracturing : new proppant improves fracture conductivity. In: SPE Annual Technical Conference and Exhibition.
McLennan, J.D., Green, S.J., Bai, M., 2008. Proppant placement during tight gas shale stimulation: literature review and speculation. Armaghan 1–14.
Meehan, D.E.M., Shah, S.N., Services, H., 1991. Static Proppant-Settling Characteristics of Non-newtonian Fracturing Fluids in a Large-Scale Test Model (August).
Mobbs, A., Hammond, P., 2001. Computer simulations of proppant transport in a hydraulic fracture. SPE Prod. Facil. 16 (2), 8–10.
Mokryakov, V., 2011. Analytical Solution for Propagation of Hydraulic Fracture with Barenblatt ' S Cohesive Tip Zone, pp. 159–168.
Moukalled, F., Mangani, L., Darwish, M., 2016. The Finite Volume Method in Computational Fluid Dynamics, Volume 113 *of Fluid Mechanics And its Applications*. Springer International Publishing.
Mountrakis, L., Lorenz, E., Hoekstra, A.G., 2014. Validation of an efficient two-dimensional model for dense suspensions of red blood cells. Int. J. Mod. Phys. C 25 (12), 1441005.
Nicodemo, L., Nicolais, L., Landel, R., 1974. Shear rate dependent viscosity of suspensions in Newtonian and non-Newtonian liquids. Chem. Eng. Sci. 29 (3), 729–735.
Novotny, E., 1977. Proppant transport. In: SPE Annual Fall Technical Conference and Exhibition. Society of Petroleum Engineers.
Obeysekara, A., 2018. Numerical Modelling of Hydraulic Fracturing in Naturally Fractured Rock. Thesis.
Onate, E., Rojek, J., 2004. Combination of discrete element and finite element methods for dynamic analysis of geomechanics problems. Comput. Methods Appl. Mech. Eng. 193 (27–29), 3087–3128.
Osiptsov, A.A., 2017. Fluid mechanics of hydraulic fracturing : a review. J. Petrol. Sci. Eng. 156 (May), 513–535.
Ouyang, S., Carey, G.F., Yew, C.H., 1997. An adaptive finite element scheme for hydraulic fracturing with proppant transport. Int. J. Numer. Methods Fluid. 24 (7), 645–670.
Palisch, T., Al-Tailji, W., Bartel, L., Cannan, C., Zhang, J., Czapski, M., Lynch, K., 2017. Far-field proppant detection using electromagnetic methods -latest field results. In: SPE Hydraulic Fracturing Technology Conference and Exhibition volume Day 1 Tue, January 24, 2017, D011S001R001.
Pangilinan, K.D., Leon, A.C.C.D., Advincula, R.C., 2016. Polymers for proppants used in hydraulic fracturing Polymers for proppants used in hydraulic fracturing. J. Petrol. Sci. Eng.
Panton, R., 1996. Incompressible Flow. Wiley.
Patankar, N., Joseph, D., Wang, J., Barree, R., Conway, M., Asadi, M., 2002. Power law correlations for sediment transport in pressure driven channel flows. Int. J. Multiphas. Flow 28 (8), 1269–1292.
Pearson, J., 1994. On suspension transport in a fracture: framework for a global model. J. Non-Newtonian Fluid Mech. 54 (C), 503–513.
Perkins, T., Kern, L., 1961. Widths of hydraulic fractures. J. Petrol. Technol. 13 (9), 937–949, 0.
Prosperetti, A., Tryggvason, G., 2009. Computational Methods for Multiphase Flow. Cambridge University Press.
Rahim, Z., Holditch, S.A., 1992. The Effects of Mechanical Properties and Selection of Completion Interval upon the Created and Propped Fracture Dimensions in Layered Reservoirs. Volume SPE-24349-MS. Society of Petroleum Engineers.
Rahim, Z., Holditch, S.A., Zuber, M.D., Buehring, D., 1995. Evaluation of fracture treatments using a layered reservoir description: field examples. J. Petrol. Sci. Eng. 12 (4), 257–267.
Rahman, M.M., Rahman, M.K., 2010. A review of hydraulic fracture models and development of an improved Pseudo-3D model for stimulating tight oil/gas sand. Energy Sources, Part A Recovery, Util. Environ. Eff. 32 (15), 1416–1436.
Raimbay, A., Babadagli, T., Kuru, E., Develi, K., 2016. Quantitative and visual analysis of proppant transport in rough fractures. J. Nat. Gas Sci. Eng. 33, 1291–1307.
Roostaei, M., Nouri, A., Fattahpour, V., Chan, D., 2018. Numerical simulation of proppant transport in hydraulic fractures. J. Petrol. Sci. Eng. 163 (December 2017), 119–138.
Sahai, R., Moghanloo, R.G., 2019. Proppant transport in complex fracture networks – a review. J. Petrol. Sci. Eng. 182, 106199.
Shah, S.N., 1982. Proppant settling correlations for non-Newtonian fluids under static and dynamic conditions. Soc. Petrol. Eng. J. 22 (2), 164–170, 0.
Shields, I.A., 1936. Application of similarity principles and turbulence research to bed-load movement. J. Hydraul. Eng.
Shiozawa, S., McClure, M., 2016. Simulation of proppant transport with gravitational settling and fracture closure in a three-dimensional hydraulic fracturing simulator. J. Petrol. Sci. Eng. 138, 298–314.
Shook, C., Roco, M., 1991. Slurry Flow: Principles and Practice, first ed. Elsevier.
Siddhamshetty, P., Mao, S., Wu, K., Kwon, J.S.-I., 2020. Multi-size proppant pumping schedule of hydraulic fracturing: application to a mp-pic model of unconventional reservoir for enhanced gas production. Processes 8 (5), 570.

Smith, M.B., Bale, A., Britt, L.K., Hainey, B.W., Klein, H.K., 1997. Enhanced 2d Proppant Transport Simulation: the Key to Understanding Proppant Flowback and Post-frac Productivity. Volume SPE-38610-MS. Society of Petroleum Engineers.
Suri, Y., Islam, S.Z., Hossain, M., 2019. A new CFD approach for proppant transport in unconventional hydraulic fractures. J. Nat. Gas Sci. Eng. 70 (July), 102951.
Suri, Y., Islam, S.Z., Hossain, M., 2020a. Effect of fracture roughness on the hydrodynamics of proppant transport in hydraulic fractures. J. Nat. Gas Sci. Eng. 80, 103401.
Suri, Y., Islam, S.Z., Hossain, M., 2020b. Numerical modelling of proppant transport in hydraulic fractures. Fluid Dynam. Mater. Process. 16, 297–337.
Thomas, D.G., 1965. Transport characteristics of suspension: VIII. A note on the viscosity of Newtonian suspensions of uniform spherical particles, 277, 267–277.
Tomac, I., Gutierrez, M., 2015. Micromechanics of proppant agglomeration during settling in hydraulic fractures. J. Petrol. Explorat. Product. Technol. 5 (4), 417–434.
Tong, S., Mohanty, K.K., 2016. Proppant transport study in fractures with intersections. Fuel 181, 463–477.
Tsai, K., Fonseca, E.R., Degaleesan, S., Lake, E., 2012. Advanced computational modeling of proppant settling in water fractures for shale gas production. In: *SPE Hydraulic Fracturing Technology Conference*, Volume All Days. SPE-151607-MS.
Tsuo, Y.P., Gidaspow, D., 1990. Computation of flow patterns in circulating fluidized beds. AIChE J. 36 (6), 885–896.
Vandamme, L., Curran, J.H., 1989. A three-dimensional hydraulic fracturing simulator. Int. J. Numer. Methods Eng. 28 (4), 909–927.
Vandamme, L., Detournay, E., Cheng, A.H.-D., 1989. A two-dimensional poroelastic displacement discontinuity method for hydraulic fracture simulation. Int. J. Numer. Anal. Methods GeoMech. 13 (2), 215–224.
Wahl, H., Campbell, J., 1963. Sand movement in horizontal fractures. J. Petrol. Technol. 15 (11).
Wang, J., Elsworth, D., Denison, M.K., 2018a. Hydraulic fracturing with leakoff in a pressure-sensitive dual porosity medium. Int. J. Rock Mech. Min. Sci. 107, 55–68. July 2017.
Wang, J., Elsworth, D., Denison, M.K., 2018b. Propagation, proppant transport and the evolution of transport properties of hydraulic fractures. J. Fluid Mech. 855, 503–534.
Wang, X., Yao, J., Gong, L., Sun, H., Yang, Y., Zhang, L., Li, Y., Liu, W., 2019. Numerical simulations of proppant deposition and transport characteristics in hydraulic fractures and fracture networks. J. Petrol. Sci. Eng. 183, 106401.
Weng, X., Kresse, O., Chuprakov, D., Cohen, C.-E., Prioul, R., Ganguly, U., 2014. Applying complex fracture model and integrated workflow in unconventional reservoirs. J. Petrol. Sci. Eng. 124, 468–483.
Wilcock, P.R., Crowe, J.C., 2003. Surface-based transport model for mixed-size sediment. J. Hydraul. Eng. 129 (2), 120–128.
Wu, C.-H., Yi, S., Sharma, M.M., 2017. Proppant distribution among multiple perforation clusters in a horizontal wellbore. In: SPE Hydraulic Fracturing Technology Conference and Exhibition volume Day 1 Tue, January 24, 2017, D011S002R002.
Wu, H., Madasu, S., Lin, A., 2014. A computational model for simulating proppant transport in wellbore and fractures for unconventional treatments. In: Abu Dhabi International Petroleum Exhibition and Conference. Society of Petroleum Engineers.
Zeng, J., Li, H., Zhang, D., 2016. Numerical simulation of proppant transport in hydraulic fracture with the upscaling CFD-DEM method. J. Nat. Gas Sci. Eng. 33, 264–277.
Zeng, J., Li, H., Zhang, D., 2019. Numerical simulation of proppant transport in propagating fractures with the multi-phase particle-in-cell method. Fuel 245, 316–335.
Zhang, G., Gutierrez, M., Li, M., 2017a. Numerical simulation of transport and placement of multi-sized proppants in a hydraulic fracture in vertical wells. Granul. Matter 19 (2), 32.
Zhang, G., Li, M., Gutierrez, M., 2017b. Numerical simulation of proppant distribution in hydraulic fractures in horizontal wells. J. Nat. Gas Sci. Eng. 48, 157–168.
Zoveidavianpoor, M., Gharibi, A., 2015. Application of polymers for coating of proppant in hydraulic fracturing of subterraneous formations: a comprehensive review. J. Nat. Gas Sci. Eng. 24, 197–209.